2023 21st IEEE Interregional NEWCAS Conference (NEWCAS) | 979-8-3503-0024-6/23/$31.00 ©2023 IEEE | DOI: 10.1109/NEWCAS57931.2023.10198039

Heterogeneity in Time Delays between Mutually Synchronized 24 GHz Oscillators

Christian Hoyer*†, Lucas Wetzel‡§, Dimitris Prousalis‡, Jens Wagner*¶, Frank Jülicher‡, Frank Ellinger*¶
*Chair for Circuit Design and Network Theory, Technische Universität Dresden, Germany
¶Centre for Tactile Internet with Human-in-the-Loop (CeTI), Technische Universität Dresden, Germany
‡Max Planck Institute for the Physics of Complex Systems, Dresden, Germany
†christian.hoyer1@tu-dresden.de, §lwetzel@pks.mpg.de

***Abstract*—This paper presents the analysis and measurements of the effects of heterogeneous cross-coupling time delays on synchronized states in a network of mutually coupled oscillators. In a network of three mutually coupled phase-locked loops, operating at 24 GHz in a chain topology, the phase relations and frequency of the synchronized state are quantified. The measurements show that such delay heterogeneity changes the properties of self-organized synchronized states. Specifically, it reduces the range of frequencies over which self-organized synchronous states form. It is observed that the frequency of the self-organized synchronized state that would form over a sub-network of two oscillators alone, lies within this range. The experimental observations presented here reveal new insights into the effects of heterogeneity on the dynamics of self-organization in mutually delay-coupled oscillators and the implications for the properties of synchronized states.**

***Index Terms*—synchronization, delay effects, phase locked loops, oscillator, delays, couplings, frequency synchronization, delay coupling.**

I. Introduction

Synchronization of distributed sensor networks plays a critical role in various applications, including localization and tracking with radar sensors [1]–[3], industrial automation for monitoring and control of facilities [4], [5], and body area sensor networks for human-machine interaction [6]. The challenge arises in any network where sensors are wirelessly connected, and especially when they are moving, as this can introduce arbitrary time delays between them, making synchronization difficult. Biologically inspired techniques, such as those based on the flashing of fireflies [7]–[10], can provide a flexible and robust solution for synchronizing distributed sensor networks. One implementation of such a technique is the mutual synchronization of time-delayed coupled oscillators [11]–[13]. In this approach, the individual nodes are mutually coupled in a flat hierarchy. This means that there is no hierarchical master-slave concept and synchronization is achieved by very complex self-organized dynamics of the network.

The concept of mutual synchronization has been studied extensively since the 1960s [11], [14]–[16]. Early studies focused on the coupling of oscillators without including the time delay between nodes [17]. Later models consider the time delay, but use linearized models that are valid only for time delays in the order of the coupling frequency [18]–[20]. In more recent studies, the individual nodes are represented as phase-locked loops (PLL) and the nonlinearity of individual components is also taken into account [21]–[27]. Thus, it is possible to study the complex dynamics of delay-coupled oscillator systems.

In [28], the effect of heterogeneity as an asymmetric time delay between two coupled oscillators was analyzed and it was shown that the phase differences depend monotonically on the difference of the time delays. [29] extends this analysis to four fully digital delay-coupled PLLs connected in a ring topology. Here, the mean of the time delays between the nodes was kept constant so that only the phase differences are affected. By defining a critical time delay, as presented in [30], a maximum time delay between two coupled oscillators can be identified at which stable synchronization can be achieved.

The goal of this paper is to investigate the effects of heterogeneity in the time delays between three mutually coupled PLLs. In this minimal example, all nodes are connected in a chain topology and the mean time delay between the nodes is varied. To understand the details of varying time delays between coupled nodes, the model used for delay-coupled oscillators is briefly studied with respect to time delay heterogeneities in Section II. Section III presents the hardware and measurement setup used for the measurements presented in Section IV.

II. Model of Time-Delayed Coupled PLL Nodes

In a system of mutually delay-coupled PLL nodes, a stable synchronized state for a given time delay configuration is characterized by equal output frequencies of the nodes and constant phase differences over time. Such states can be predicted using a dynamical model [13], [24]–[26]. Assuming that in a synchronized state all perturbations have decayed and that all nodes in the network are identical, the dynamical model representing any node k in the network is given by the following set of implicit expressions

$$\mathrm{N}\,\Omega_{\mathrm{NET}} = \omega_0 + \mathrm{G_{PD}}\,\mathrm{G_{LF}}\,\mathrm{K_{VCO}} \times \frac{1}{\mathrm{E}_k}\sum_{i=1}^{\mathrm{M}} d_{ki} \triangle \left[-\Omega_{\mathrm{NET}}\,\tau_{\mathrm{delay},ki} - \Delta\varphi_{ki} + \varphi_{\mathrm{fb}}\right]. \tag{1}$$

Here, N denotes the frequency division factor, Ω_{NET} the divided angular output frequency of each node in the synchronized state, ω_0 the free-running closed-loop frequency

of the node, $\mathrm{G_{PD}}$ the steady state gain of the phase detector (PD), $\mathrm{G_{LF}}$ the steady state gain of the loop filter (LF), $\mathrm{K_{VCO}}$ the sensitivity of the voltage controlled oscillator (VCO) at the operating point, E_k the number of external inputs to a node k, M the number of PLL nodes in the network, d_{ki} the adjacency matrix parameter, which is either 1 or 0 depending on whether node k and i are coupled or not, $\triangle(\cdot)$ the normalized phase-error transfer function of an XOR based phase detector, $\tau_{\mathrm{delay},ki}$ the cross-coupling time delay, φ_{fb} feedback path phase shift, and $\Delta\varphi_{ki}$ denotes the phase difference between nodes k and i in the synchronized state.

Synchronized states that can exist in such networks fulfill Eq. 1. However, only stable states can be observed in measurements. Hence, their response to phase perturbations needs to be analyzed. However, due to the nonlinear coupling function and implicit nature of the equations, it is difficult to obtain the unknown $\Delta\varphi_{ki}$ and Ω_{NET} analytically. Previous research [20], [22], [25] has shown that for certain conditions there can be a constant *mode-locking phase difference* $\Delta\varphi_{\mathrm{mode},ki}$. For delay-coupled oscillators in a linear chain, i.e., open boundary conditions with equal time delay between nodes, this phase difference is either 0 or π. This is due to the periodic characteristics of the phase detector [25], [26] and allows the prediction of synchronized states for equal time delays between nodes.

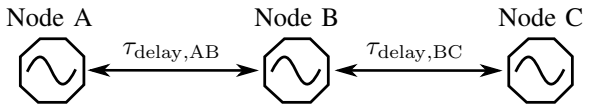

Fig. 1. Three mutually time-delayed coupled PLL nodes where the time delay between node A and B corresponds to $\tau_{\mathrm{delay,AB}} = \tau_{\mathrm{delay,BA}}$ and between node B and C to $\tau_{\mathrm{delay,BC}} = \tau_{\mathrm{delay,CB}}$.

The network considered consists of three nodes A, B, and C connected in a chain topology as shown in Fig. 1. The time delay between nodes A and B is $\tau_{\mathrm{delay,AB}}$ and between B and C is $\tau_{\mathrm{delay,BC}}$. The time delays between two nodes are equal in both directions. From Eq. 1 an equation for each node can be written

$$\mathrm{N}\,\Omega_{\mathrm{NET}} = \omega_0 + \mathrm{G_{PD}}\,\mathrm{G_{LF}}\,\mathrm{K_{VCO}} \times \triangle\left[-\Omega_{\mathrm{NET}}\,\tau_{\mathrm{delay,AB}} - \Delta\varphi_{\mathrm{AB}}\right], \tag{2}$$

$$\mathrm{N}\,\Omega_{\mathrm{NET}} = \omega_0 + \mathrm{G_{PD}}\,\mathrm{G_{LF}}\,\mathrm{K_{VCO}} \times \frac{1}{2}\left(\triangle\left[-\Omega_{\mathrm{NET}}\,\tau_{\mathrm{delay,AB}} + \Delta\varphi_{\mathrm{AB}}\right] + \triangle\left[-\Omega_{\mathrm{NET}}\,\tau_{\mathrm{delay,BC}} - \Delta\varphi_{\mathrm{BC}}\right]\right), \tag{3}$$

$$\mathrm{N}\,\Omega_{\mathrm{NET}} = \omega_0 + \mathrm{G_{PD}}\,\mathrm{G_{LF}}\,\mathrm{K_{VCO}} \times \triangle\left[-\Omega_{\mathrm{NET}}\,\tau_{\mathrm{delay,BC}} + \Delta\varphi_{\mathrm{BC}}\right]. \tag{4}$$

These implicit equations with the nonlinear phase-error transfer function $\triangle(\cdot)$ can be solved numerically to obtain the unknowns Ω_{NET}, $\Delta\varphi_{\mathrm{AB}}$ and $\Delta\varphi_{\mathrm{BC}}$. An inversion of the signal in the feedback path can be accounted for by adding a phase shift of $\varphi_{\mathrm{fb}} = \pi$ in the argument of $\triangle(\cdot)$.

III. Hardware and Measurement Setup

To study the effects of time delay heterogeneity between coupled nodes, three identical PLL nodes as presented in [26], [30] and [31] are used. These nodes have four input and output channels that provide a low-voltage positive emitter-coupled logic (LVPECL) interface to allow coupling to other nodes directly, or via programmable delay line modules. These delay modules consist of four cascaded programmable delay chips that allow the total delay to be set between $11.2\,\mathrm{ns}$ and $52\,\mathrm{ns}$. These delays can be programmed at runtime via USB for each direction and for each module individually.

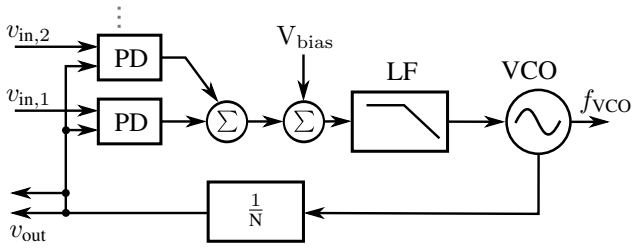

Fig. 2. Block diagram of the PLL node for mutual synchronization. Here two input and output channels are used, all other unused channels are disabled and marked by gray dots.

The architecture of the PLL is shown in the block diagram in Fig. 2. In this paper, only two input and output channels are used, as indicated by the input voltages $v_{\mathrm{in},i}$, where i denotes the corresponding channel. Each channel consists of an XOR-based phase detector (PD) with sensitivity of $\mathrm{G_{PD}} = 0.8$ whose output is weighted in a subsequent summing circuit. Prior to filtering in a loop filter (LF), the summed signal is shifted by a constant voltage $\mathrm{V_{bias}}$. It compensates for any component tolerances, such as different VCO tuning characteristics or op-amp output voltages, so that each node has approximately the same free-running frequency. The VCO sensitivity $\mathrm{K_{VCO}}$ at the operating point is $921.63\,\mathrm{MHz\,V^{-1}}$. A cascaded second-order RC filter with a cutoff frequency of $398.1\,\mathrm{kHz}$ and $\mathrm{G_{LF}} = 1$ is used for the LF. The output and cross-coupling signal v_{out} of the PLL is the output signal of the VCO divided by the factor $\mathrm{N} = 512$. The signal of the node's feedback path is inverted, i.e., $\varphi_{\mathrm{fb}} = \pi$.

To validate the predicted synchronized states, the output signals v_{out} of each node are measured with an oscilloscope, as shown in the scheme of the measurement setup in Fig. 3. The frequency and the phase difference between the nodes

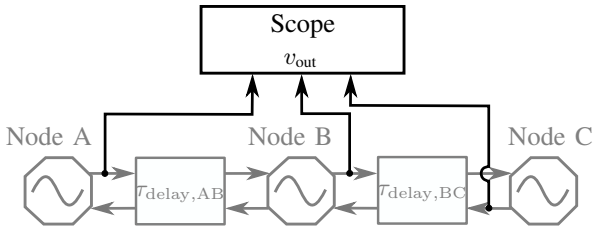

Fig. 3. Measurement setup with three mutually delay-coupled PLL nodes for capturing the cross-coupling frequencies as well as the phase differences between nodes.

are extracted using the automated measurement functions of the Rohde & Schwarz RTO 2044 oscilloscope. For calibration of all free-running closed-loop oscillator frequencies, an additional spectrum analyzer was used, which was connected to the high-frequency output of the PLL node. All PLL nodes were calibrated to a free-running frequency of 23.5 GHz by adjusting V_{bias}. The maximum deviation between the individual PLL nodes is below 2 MHz. The spectrum of all coupled oscillators is measured using a time signal captured at the high frequency outputs on a Keysight UXR1004 real-time oscilloscope, followed by an FFT. A photo of the measurement setup is shown in Fig. 4. When setting the delays of each individual delay module via USB, the fixed delay is set first, the variable delay subsequently.

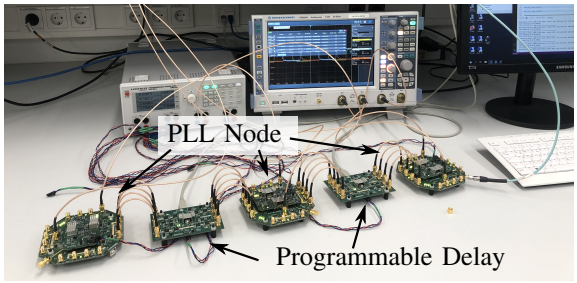

Fig. 4. Photo of the measurement setup in the laboratory where three nodes are mutually coupled in a chain network topology. The equipment used starting from the left: power supply and oscilloscope.

IV. Measurement

Three aspects are analyzed quantitatively and qualitatively to study heterogeneous time delays between mutually coupled oscillators. First, the two time delays are linearly increased simultaneously. Then, one of the time delays is set to a fixed value while the other is varied linearly. This changes the mean delay in the network. Finally, the spectrum of all three nodes and heterogeneous time delays is measured. During the delay-sweep over the range covered by the delay modules, all nodes remain coupled. For each delay value visited during the sweep, at least 150 individual measurements of phase differences and output frequencies are captured.

Fig. 5 shows the measurement and model predictions for equal time delays $\tau_{\mathrm{delay,AB}} = \tau_{\mathrm{delay,BC}} = \tau_{\mathrm{delay}}$ between the three nodes. For each delay measured, a stable synchronized state can be observed. The measured network frequency f_{NET} of all nodes, shown in Fig. 5(a), has a mean standard deviation of 35.89 kHz. The theoretical predictions for the mode-locking phase differences between nodes are in good agreement with the measurements. The corresponding phase differences $\Delta\varphi_{ki}$ are plotted in Fig. 5(b). It can be seen that the phase differences $\Delta\varphi_{\mathrm{AB}}$ as well as $\Delta\varphi_{\mathrm{BC}}$ are close to the theoretical results with the expected mode locking phase difference $\Delta\varphi_{\mathrm{mode},ki}$ of 0 (in-phase) or π (anti-phase). As the time delay increases, there is a monotonically linear decrease in the phase differences $\Delta\varphi_{\mathrm{AB}}$ and $\Delta\varphi_{\mathrm{BC}}$, e.g. from about 200° at 33 ns to about 160° at 44 ns. The phase differences $\Delta\varphi_{\mathrm{AC}} = \Delta\varphi_{\mathrm{AB}} + \Delta\varphi_{\mathrm{BC}}$ is close to in-phase for all time delays analyzed.

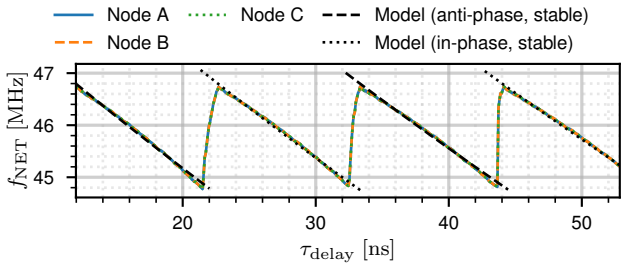

(a) Network frequency f_{NET} of all nodes.

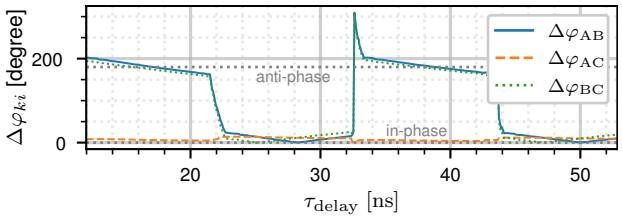

(b) Phase difference $\Delta\varphi_{ki}$ between nodes.

Fig. 5. Model results and measurements of synchronized states in a network of three mutually coupled nodes in chain topology for identical increasing cross-coupling time delays $\tau_{\mathrm{delay,AB}} = \tau_{\mathrm{delay,BC}} = \tau_{\mathrm{delay}}$.

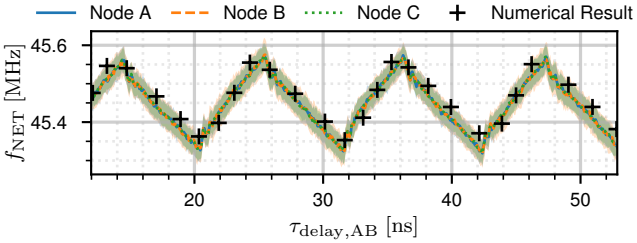

(a) Network frequency f_{NET} of all nodes.

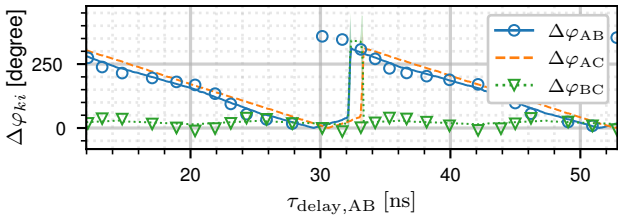

(b) Phase difference $\Delta\varphi_{ki}$ between nodes.

Fig. 6. Measured synchronized states in a network of three mutually coupled nodes in chain topology for increasing cross-coupling time delays $\tau_{\mathrm{delay,AB}}$ and fixed time delay $\tau_{\mathrm{delay,BC}}$ of 30 ns. The standard deviation of both quantities for a minimum of 150 measurements is shown in shaded colors. The numerical solution to the set of implicit Eq. 2-Eq. 4 are denoted by markers. Note that more solutions can exist and the total node gain was fitted to the measurements using a factor of 0.25.

The measured results for heterogeneous time delays between coupled nodes, i.e. $\tau_{\mathrm{delay,AB}} \neq \tau_{\mathrm{delay,BC}}$ are shown in Fig. 6. Here $\tau_{\mathrm{delay,BC}}$ has a constant value of 30 ns and $\tau_{\mathrm{delay,AB}}$ is linearly increased. The shape observed from the measured frequency of the coupled nodes in Fig. 6(a) is a triangular function that depends on the time delay $\tau_{\mathrm{delay,AB}}$ and alternates between 45.58 MHz and 45.12 MHz. The standard deviation is shown in shaded colors for each node respectively, it's maximum value for all delays and nodes is 36.33 kHz. From the phase difference in Fig. 6(b), it can be

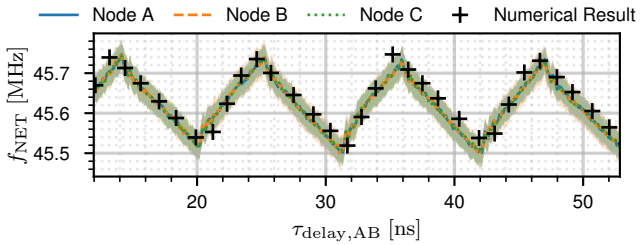

(a) Network frequency f_{NET} of all nodes.

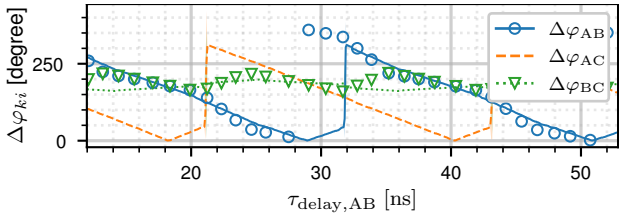

(b) Phase difference $\Delta\varphi_{ki}$ between nodes.

Fig. 7. Measured synchronized states in a network of three mutually nodes in chain topology for increasing cross-coupling time delays $\tau_{\mathrm{delay,AB}}$ and fixed time delay $\tau_{\mathrm{delay,BC}}$ of 40 ns. Presented in the same way as in Fig. 6.

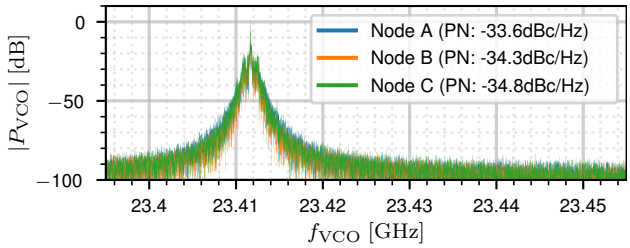

Fig. 8. Measured normalized power spectral densities and phase noise level (PN) at an offset of 1 MHz from the carrier for three mutually coupled PLL nodes in chain topology for a time delay $\tau_{\mathrm{delay,AB}}$ of 50 ns and $\tau_{\mathrm{delay,BC}}$ of 30 ns. The frequency f_{VCO} of all nodes is at 23.412 GHz.

observed that $\Delta\varphi_{\mathrm{BC}}$ between the two coupled nodes with fixed delay is constant and close to in-phase for all $\tau_{\mathrm{delay,AB}}$. The difference $\Delta\varphi_{\mathrm{AB}}$ is monotonically decreasing with respect to the linearly changing time delay. The average standard deviation of the phase difference $\Delta\varphi_{ki}$ for all delays over all nodes is 1.67°. The numerical results for both cases with fixed time delay agree well with the measurements. However, there is an additional fitting factor of 0.25 that needs to be further analyzed to fully understand the overall dynamics.

For a fixed time delay $\tau_{\mathrm{delay,BC}}$ of 40 ns, the frequencies and phase difference between nodes are plotted in Fig. 7. Like the previous measurement, the frequency shows a similar shape, with frequencies between 45.75 MHz and 45.5 MHz for all time delays studied. The maximum standard deviation is 34.68 kHz. The phase difference $\Delta\varphi_{\mathrm{BC}}$, associated to the fixed time delay is close to anti-phase. The phase difference $\Delta\varphi_{\mathrm{AB}}$ of the variable delay decreases again in a linear manner as the time delay $\tau_{\mathrm{delay,AB}}$ increases. The average standard deviation of the phase difference across all nodes and delays is 1.20°.

The measured spectrum of the high frequency outputs of each node for a delay $\tau_{\mathrm{delay,AB}}$ of 50 ns and $\tau_{\mathrm{delay,BC}}$ of 30 ns is shown in Fig. 8. The frequency of all nodes is identical at 23.412 GHz. The FFT function resolution bandwidth is 3.82 kHz. The overall form of all three spectra overlaps and has an almost identical shape. The measured phase noise at an offset frequency of 1 MHz to the carrier is −33.63 dBc/Hz, −34.34 dBc/Hz and −34.78 dBc/Hz for node A, B and C. The system presented is not optimized for low phase noise.

V. Conclusion and Discussion

The results presented in this paper show how the properties of self-organized synchronized states are affected by heterogeneous time delays in a network of mutually delay-coupled phase-locked loops (PLLs). For identical time delays, in- and anti-phase synchronized states, i.e., phase difference 0 or π, can be observed in networks with open-boundary conditions. For the three mutually delay-coupled PLL nodes $\{\mathrm{A},\mathrm{B},\mathrm{C}\}$ in a chain topology studied here, the phase-difference between the oscillator pair $\{\mathrm{B},\mathrm{C}\}$ is – depending on the value of the fixed time delay – either close to 0 or π, while the phase difference between the pair $\{\mathrm{A},\mathrm{B}\}$ changes linearly as the cross-coupling time delay is increased. In consequence, the phase-difference between pair $\{\mathrm{A},\mathrm{C}\}$ is almost equal or shifted by π to that of pair $\{\mathrm{A},\mathrm{B}\}$. Hence, the phase-difference between the pair $\{\mathrm{B},\mathrm{C}\}$ with fixed cross-coupling time delay is only slightly affected by the change of the time delay between pair $\{\mathrm{A},\mathrm{B}\}$. If the time delays between the pairs $\{\mathrm{A},\mathrm{B}\}$ and $\{\mathrm{B},\mathrm{C}\}$ are identical, the original state for identical time delays is recovered. In addition, it can be observed that the frequencies of the synchronized states for fixed time delay are in a range around the frequency of the network with identical time delay at that given fixed delay. For example, for a delay of 30 ns, the synchronized state of the network with identical time delay has a frequency of 45.35 MHz. For different time delays, the frequency is between 45.58 MHz and 45.32 MHz. The frequency shows a triangular characteristic as a function of the time delay between the pair $\{\mathrm{A},\mathrm{B}\}$, which can only be associated to the characteristic of the phase detector. The measurements and observations of the effect of time delay heterogeneity between mutually delay-coupled oscillators raises the questions about the internal dynamics of sub-networks with different time delays and their effect on stable synchronized states over the entire network. However, the results and insights presented in this paper have the potential to inform future research and advancements in this area, ultimately contributing to the design and optimization of more applicable networks of mutually delay-coupled PLLs.

Acknowledgment

For support and cooperation we would like to thank the BMBF (Federal Ministry of Education and Research) projects PLL-Synchronisation (Grant 03VP06432), 6G-life (Grant 16KISK001K) and E4C (Grant 16ME0426K), and the DFG (German Research Foundation) Cluster of Excellence “Center for Tactile Internet with Human-in-the-Loop” (CeTI) with project ID 390696704.

References

[1] M. Göttinger, M. Hoffmann, M. Christmann, M. Schutz, F. Kirsch, P. Gulden, and M. Vossiek, "Coherent Automotive Radar Networks: The Next Generation of Radar-Based Imaging and Mapping," *IEEE Journal of Microwaves*, vol. 1, no. 1, pp. 149–163, Jan. 2021.

[2] R. Thomä, T. Dallmann, S. Jovanoska, P. Knott, and A. Schmeink, "Joint communication and radar sensing: An overview," in *2021 15th European Conference on Antennas and Propagation (EuCAP)*. IEEE, Mar. 2021.

[3] J. A. Zhang, M. L. Rahman, K. Wu, X. Huang, Y. J. Guo, S. Chen, and J. Yuan, "Enabling Joint Communication and Radar Sensing in Mobile Networks—A Survey," *IEEE Communications Surveys & Tutorials*, vol. 24, no. 1, pp. 306–345, Oct. 2022.

[4] J. Yang, J. Zhou, Z. Lv, W. Wei, and H. Song, "A Real-Time Monitoring System of Industry Carbon Monoxide Based on Wireless Sensor Networks," *Sensors*, vol. 15, no. 11, pp. 29 535–29 546, Nov. 2015.

[5] M. Wollschlaeger, T. Sauter, and J. Jasperneite, "The Future of Industrial Communication: Automation Networks in the Era of the Internet of Things and Industry 4.0," *IEEE Industrial Electronics Magazine*, vol. 11, no. 1, pp. 17–27, Mar. 2017.

[6] J. Wagner, H. Morath, J. Zhang, F. Wieczorek, L. Luneburg, F. H. P. Fitzek, and G. T. Nguyen, "Tactile Electronics Meets Softwarised Networks," in *2022 IEEE 19th Annual Consumer Communications & Networking Conference (CCNC)*. IEEE, Jan. 2022.

[7] G. Werner-Allen, G. Tewari, A. Patel, M. Welsh, and R. Nagpal, "Firefly-inspired sensor network synchronicity with realistic radio effects," in *Proceedings of the 3rd international conference on Embedded networked sensor systems*. ACM, Nov. 2005.

[8] O. Babaoglu, T. Binci, M. Jelasity, and A. Montresor, "Firefly-inspired Heartbeat Synchronization in Overlay Networks," in *First International Conference on Self-Adaptive and Self-Organizing Systems (SASO 2007)*. IEEE, Jul. 2007.

[9] K. P. O'Keeffe, H. Hong, and S. H. Strogatz, "Oscillators that sync and swarm," *Nature Communications*, vol. 8, no. 1, Nov. 2017.

[10] K. O'Keeffe and C. Bettstetter, "A review of swarmalators and their potential in bio-inspired computing," in *Micro- and Nanotechnology Sensors, Systems, and Applications XI*, M. S. Islam and T. George, Eds. SPIE, May 2019.

[11] M. Karnaugh, "A Model for the Organic Synchronization of Communications Systems," *Bell System Technical Journal*, vol. 45, no. 10, pp. 1705–1735, Dec. 1966.

[12] W. Lindsey, F. Ghazvinian, W. Hagmann, and K. Dessouky, "Network synchronization," *Proc. IEEE*, vol. 73, no. 10, pp. 1445–1467, Oct. 1985.

[13] L. Wetzel, D. J. Jörg, A. Pollakis, W. Rave, G. Fettweis, and F. Jülicher, "Self-organized synchronization of digital phase-locked loops with delayed coupling in theory and experiment," *PLOS ONE*, vol. 12, no. 2, Feb. 2017.

[14] M. B. Brilliant, "The Determination of Frequency in Systems of Mutually Synchronized Oscillators," *Bell System Technical Journal*, vol. 45, no. 10, pp. 1737–1748, Dec. 1966.

[15] A. Gersho and B. J. Karafin, "Mutual Synchronization of Geographically Separated Oscillators," *Bell System Technical Journal*, vol. 45, no. 10, pp. 1689–1704, Dec. 1966.

[16] H. Inose, H. Fujisaki, and T. Saito, "Theory of mutually synchronised systems," *Electronics Letters*, vol. 2, no. 3, p. 96, Mar. 1966.

[17] J. R. Pierce, "Synchronizing Digital Networks," *Bell System Technical Journal*, vol. 48, no. 3, pp. 615–636, Mar. 1969.

[18] H. Stover, "Network Timing/Synchronization for Defense Communications," *IEEE Trans. Commun.*, vol. 28, no. 8, pp. 1234–1244, Aug. 1980.

[19] W. L. M. Chie, "A survey of digital phase-locked loops," *Proceedings of the IEEE*, vol. 69, no. 4, pp. 410–431, Apr. 1981.

[20] G. Pratt and J. Nguyen, "Distributed synchronous clocking," *IEEE Trans. Parallel Distrib. Syst.*, vol. 6, no. 3, pp. 314–328, Mar. 1995.

[21] B. Ottino-Löffler and S. H. Strogatz, "Comparing the locking threshold for rings and chains of oscillators," *Physical Review E*, vol. 94, no. 6, p. 062203, Dec. 2016.

[22] S. Eydam and M. Wolfrum, "Mode locking in systems of globally coupled phase oscillators," *Physical Review E*, vol. 96, no. 5, p. 052205, Nov. 2017.

[23] D. Prousalis and L. Wetzel, "Synchronization in the presence of time delays and inertia: Stability Criteria," *Physical Review E*, vol. 105, no. 1, p. 014210, Jan. 2022.

[24] C. Hoyer, D. Prousalis, L. Wetzel, R. Riaz, J. Wagner, F. Jülicher, and F. Ellinger, "Mutual Synchronization with 24 GHz Oscillators," in *2021 IEEE International Symposium on Circuits and Systems (ISCAS)*. IEEE, May 2021.

[25] L. Wetzel, D. Prousalis, R. F. Riaz, C. Hoyer, N. Joram, J. Fritzsche, F. Ellinger, and F. Jülicher, "Network Synchronization Revisited: Time Delays in Mutually Coupled Oscillators," *IEEE Access*, vol. 10, pp. 80 027–80 045, Jul. 2022.

[26] C. Hoyer, L. Wetzel, D. Prousalis, J. Wagner, F. Jülicher, and F. Ellinger, "Stability Analysis of Mutually Synchronized Spatially Distributed 24 GHz Oscillators," in *2022 IEEE International Instrumentation and Measurement Technology Conference (I2MTC)*. IEEE, May 2022.

[27] L. Wetzel, D. Prousalis, F. Jülicher, R. Riaz, C. Hoyer, N. Joram, and F. Ellinger, "How to Implement Mutual Network Synchronization in the Presence of Large Cross-Coupling Delays," in *2022 Joint Conference of the European Frequency and Time Forum and IEEE International Frequency Control Symposium (EFTF/IFCS)*. IEEE, Apr. 2022.

[28] N. Punetha and L. Wetzel, "How clock heterogeneity affects synchronization and can enhance stability," *Physical Review E*, vol. 106, no. 5, p. 054216, Nov. 2022.

[29] ——, "Heterogeneity-induced synchronization in delay-coupled electronic oscillators," *Physical Review E*, vol. 106, no. 5, p. L052201, Nov. 2022.

[30] C. Hoyer, L. Wetzel, D. Prousalis, J. Wagner, F. Jülicher, and F. Ellinger, "Mutual Synchronization of Spatially Distributed 24 GHz Oscillators up to Distances of 500 m," *IEEE Trans. Circuits Syst. II*, vol. 69, no. 9, pp. 3689–3693, Sep. 2022.

[31] ——, "Entrainment of Mutually Synchronized Spatially Distributed 24 GHz Oscillators," *IEEE Trans. Circuits Syst. I*, pp. 1–14, Apr. 2023.